Material removal and friction behaviour in scratching of RB-SiC ceramics at elevated temperatures

Xiaoshuang rao[a,b], Feihu Zhang[a**], Xichun Luo[b*], Fei Ding[b], Yukui Cai[b], Jining Sun[c], Haitao Liu[a]

[a] *School of Mechatronics Engineering, Harbin Institute of Technology, Harbin 150001, China*

[b] *Centre for Precision Manufacturing, DMEM, University of Strathclyde, Glasgow G1 1XQ, UK*

[c] *Institute of Mechanical, Process and Energy Engineering, School of Engineering and Physical Sciences, Heriot-Watt University, Riccarton, Edinburgh EH14 4AS, UK*

[*] *Corresponding author E-mail address: *xichun.luo@strath.ac.uk; **zhangfh@hit.edu.cn*

Abstract: Thermal-assistant is considered potentially as an effective approach to improve machinability of hard and brittle materials. Understanding the material removal and friction behaviour influenced by the purposely introduced heat is crucial to obtain high quality machined surface. This paper aims to reveal material removal and friction behaviours of RB-SiC ceramics scratched by a Vickers indenter at elevated temperatures. Material removal mode, scratching hardness, critical depth of ductile-brittle transition, scratching force and friction were discussed under different penetration depths. Size effect of scratching hardness was used to assess the plastic deformation at elevated temperature. A modified model was established to predict the critical depth at elevated temperatures by taking into account of the changes of mechanical properties. The results revealed that the material deformation and adhesive behaviour enhanced the material removal in ductile regime and the coefficient of friction at elevated temperatures.

Keywords: RB-SiC ceramic, scratching, material removal, elevated temperature, friction

1 Introduction

In recent decades, reaction-bonded silicon carbide (RB-SiC) has provoked the interests of researchers because of its promising applications in lightweight space mirror, moulding dies and nuclear industry [1–3]. Strict demands on the surface integrity are put forward by these industrial applications, especially in the optics. Therefore, some thermal-assisted hybrid machining processes such as laser-assisted grinding [4] and electrical discharge diamond grinding [5] have been applied in machining of RB-SiC ceramics to obtain better surface integrity by changing the material property of the machined surface. The ductile removal regime is considered as the way to obtain a better machined surface finish [6,7] for this hard and brittle material. As a result, the friction between the tool and workpiece will also change due to the transition of the material removal mode, which may cause surface/subsurface damage. Thus, material removal and friction behaviour are crucial to surface integrity during the machining process.

Scratch technology with a single diamond grit/indenter is widely applied in the study of material removal mechanism and friction behaviours. By ploughing and cutting the surface of a weaker material, the scratching test can be used to assess the adhesion, damage, wear, strength and some other properties of the material [8]. The whole process is basically subdivided into five regimes, namely the elastic regime, the plastic regime, the subsurface cracking regime, the surface and subsurface cracking regime and the micro-abrasive regime in nanoscratching experiments [9,10]. The plastic deformation regime only occurs when stress appears on the surface of material and accumulated damages still has not emerged [11]. However, the shearing stress on the material surface during scratching is strongly influenced by the coefficient of friction [9]. Brittle material can often be removed in ductile regime rather than brittle fracture when the plastic deformation induced by the force and friction is small enough to avoid brittle fracture [12]. In scratching test, the transition from ductile to fracture behaviour is directly related to the residual groove recovery angle, initial contact radius, coefficient of friction (COF), applied load and workpiece material [13–16]. With increasing scratching load, the regime changes from smooth plastic deformation to limited cracking and even gives birth to many debris [17,18]. However, fracture is still the predominant form of damage to ceramics in most conventional processes. A large fragment of material is often removed by fracture occurred in a larger scale [19]. As a result, a higher surface roughness is achieved in brittle material removal mode [20]. The material removal mode, brittle or ductile, plays a vital role in quality control of the machined surface for machining hard and brittle material [21].

An investigation on material removal in ductile or brittle modes is the basic way to interpret material removal mechanism. However, previous researches are mainly focused on influences of scratching speed [22], scratching depths [21], repeated or multiplied scratching [23,24], grit shapes [25] and applied load [19] on material removal mode. Few reports have involved in the effects of the variation of material mechanical properties induced by process condition such as high temperatures on material removal mode. At high temperatures, i.e., above the ductile-to-brittle transition temperature, dislocations become active and assist in the plastic deformation of these nominally brittle (covalently bonded) materials [12,26]. Simultaneously, the high temperature also changes the coefficient of friction as a result of the adhesive behaviour induced by material thermal softening and oxidation [27–29]. The surface integrity will correspondently undergo some changes in these thermal-assisted machining process.

The aim of this paper is to investigate the material removal and friction behaviour of RB-SiC ceramics at elevated temperatures. Scratching tests will be conducted with a Vickers diamond indenter on an ultra-precision machine. A fibre-laser is used to generate the desired temperatures on the surface of RB-SiC specimens by setting the laser power. In order to obtain the critical information on the transition of material removal mode, all scratching tests will be performed under linearly increased penetration depths. Then, the morphology of the residual scratching grooves, scratching hardness, critical depth of ductile-brittle transition and coefficient of friction will be analyzed to investigate the deformation and friction behaviours in the scratching tests. Eventually, the influence of heat on the material removal and friction of RB-SiC ceramics are determined.

2 Details of scratching experiment

2.1 Specimen preparation

The RB-SiC ceramics from Goodfellow Cambridge Ltd. (UK) were used in the scratching test. The specimen was prepared in dimensions of 10 mm × 10 mm × 6 mm. All specimens were polished with diamond slurry of 0.25μm until surface-finish of 20 nm (Sa) was obtained. The polished specimens were then cleaned with acetone in an ultrasonic cleaner (ULTRA 8051) for 20 minutes. The X-ray diffraction result shows that the RB-SiC specimen consists of 6H-SiC, 3C-SiC and Si phases, shown in Fig.1(a). The SEM backscattered electron image reveals the microstructure of the RB-SiC specimen with SiC grains and free Si, shown in Fig.1(b). In previous work, the main mechanical properties of RB-SiC ceramic were investigated by Vickers indentation at elevated temperatures [30] and summarized in Table 1.

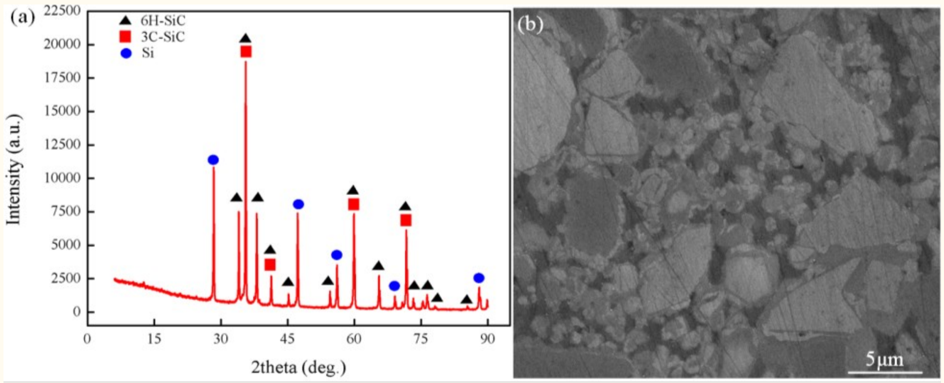

Fig 1 The XRD pattern and microstructure of RB-SiC specimen. (a) XRD result (b) SEM image

Table 1 Mechanical properties of RB-SiC ceramic at different temperatures [30]

Mechanical properties	Ambient temperature				
	Room temperature	200°C	600°C	900°C	1200°C

Vickers hardness H_v (GPa)	23.18	21.14	17.25	14.46	12.61
Elastic modulus E (GPa)	406.6	392.1	364.8	307.6	236.6
Fracture toughness K_c (MPa· m$^{1/2}$)	2.13	2.43	2.60	2.64	2.20

2.2 Experimental setup

The scratching tests were conducted with a Vickers indenter on an ultra-precision machine-micro-3D shown in Fig.2(a). The Vickers indenter, with a tip radius of 200 nm shown in Fig.2(b), was fixed on the current-controlled linear guide rail of the machine by a special clamp. The specimen was fixed in the sink of the insulating asbestine block by a bench vice. The bench vice was fastened to a dynamometer which was installed on the machine table. The Y-direction of the dynamometer was parallel to the X-axis of the machine, as shown in Fig.2 (a) and (c), which is the same direction of the scratching test. A fibre-laser (maximum power 200W) was used to heat the specimens in the scratching test. An infrared thermometer (IR-750-EUR, USA) was used to measure the temperature on the surface of RB-SiC specimen under different laser power. The relationship between the laser power and the resultant temperatures on the surface of RB-SiC specimen has been investigated in previous work [30], which showed a stable temperature can be obtained after enough heating time. Thus, all specimens were heated by the laser at different powers for sufficient time before the scratching tests to obtain the desired temperatures. In order to minimize the thermal drift caused by contact between the cold indenter and heated specimen, the Vickers indenter was simultaneously heated by keeping the specimen-indenter in contact during the heating process.

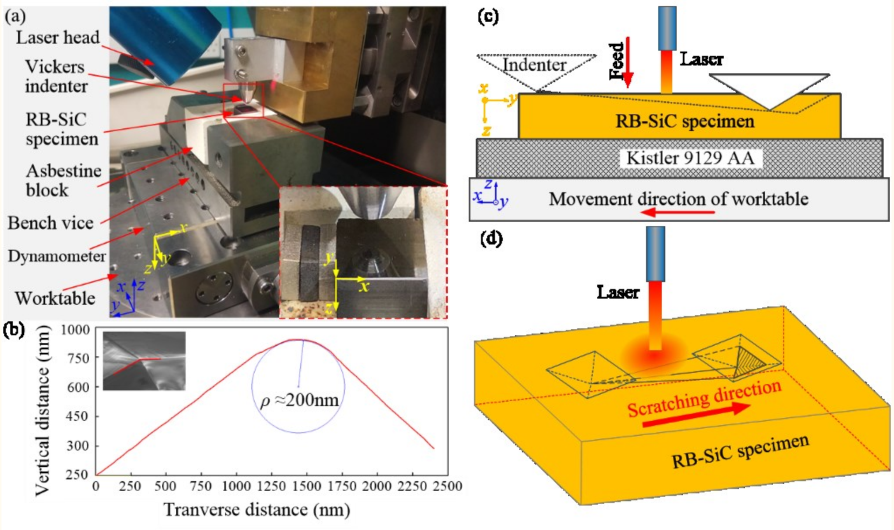

Fig.1 Illustration of scratching test at elevated temperatures. (a) Experimental setup, (b) Tip radius profile of Vickers indenter measured by AFM, (c) and (d) Schematic diagram of scratching with linearly increased depth.

In the scratching test, the scratching direction was parallel to one of the indenter diagonals and the X-axis of the machine. Considering the possible thermal expansion of the specimen during the heating process, the indenter was moved upward to a certain distance from the top surface of the RB-SiC specimen before starting the scratching test. As a result, the scratching could be certainly started from the top surface of the specimen (i.e. at a penetration depth of 0 μm), as shown in Fig.1 (c). During the scratching test, the Vickers indenter was fed downward while the worktable moved along the X-axis of the machine at the same time. In order to obtain a ramping scratching depth and keep it consistency at different temperatures, the ratio of feed rate of the Vickers indenter to the scratching speed (the velocity of the worktable movement) was kept constant. The details of the scratching parameters are listed in Table 2. For comparison, the scratching test at room temperature (RT) was also conducted.

Table 2 Details of the scratching parameters

Parameter	Value
Ambient temperature, T (℃)	RT, 200, 600, 900, 1200

Scratching speed, v_s (μm/s)	20
Ratio of indenter feed rate (v_i) to v_s	1/15
Scratching time, t (s)	30

2.3 Specimen characterization and measurement

A three-component piezoelectric dynamometer (Kistler 9129 AA) with resolution of 1mN was used to record the forces during the scratching tests. After the scratching tests, all specimens tested at different temperatures were ultrasonically cleaned for 20 minutes in acetone. Then the morphologies of the residual scratching grooves were detected by a scanning electron microscope (SEM, FEI Quanta3D FEG). The scratching lengths of different material removal regimes and the widths for the whole grooves at different temperatures were then measured by image analysis software (Digimizer, Belgium). The residual depths and heights of material pile-up along groove sides in the ductile regime were measured by an atomic force microscopy (AFM, DI Dimension 3100).

3. Results and discussion

3.1 Characteristics of scratches at different temperatures

Fig.3 shows the typical topography of the residual scratching grooves at different temperatures detected by SEM. By analogy with the finished surface with absence of cracks or few cracks defined as ductile-mode grinding in machining of zirconia ceramics [31], all scratches at different temperatures can be divided into three regimes, i.e. the ductile regime, the ductile-brittle transition (DBT) regime and the brittle regime along the scratching direction according to the different surface morphologies of the residual grooves. The scratch started with smooth surfaces and sides of the grooves at shallower penetration depth, implying the ductile regime. When the penetration depth increased, cracks and minor fracture were found on the sides of the residual grooves. Fracture was dominant on the groove sides in the brittle regime. However, the fracture tended to decrease due to the increase of temperatures, indicating the increase of ductile material removal at elevated temperatures because of thermal softening [32]. The scratching lengths of the ductile and DBT regimes increased when the temperature increased to 900°C. The reduction in ductile regime scratching length at 1200°C was attributed to the decrease of the fracture toughness with detailed discussion in Section 3.3. As a result, the corresponding critical depth of ductile-to-brittle transition may also increase when the temperature rises at the increase of penetration depth, which will also be discussed in detail in Section 3.3.

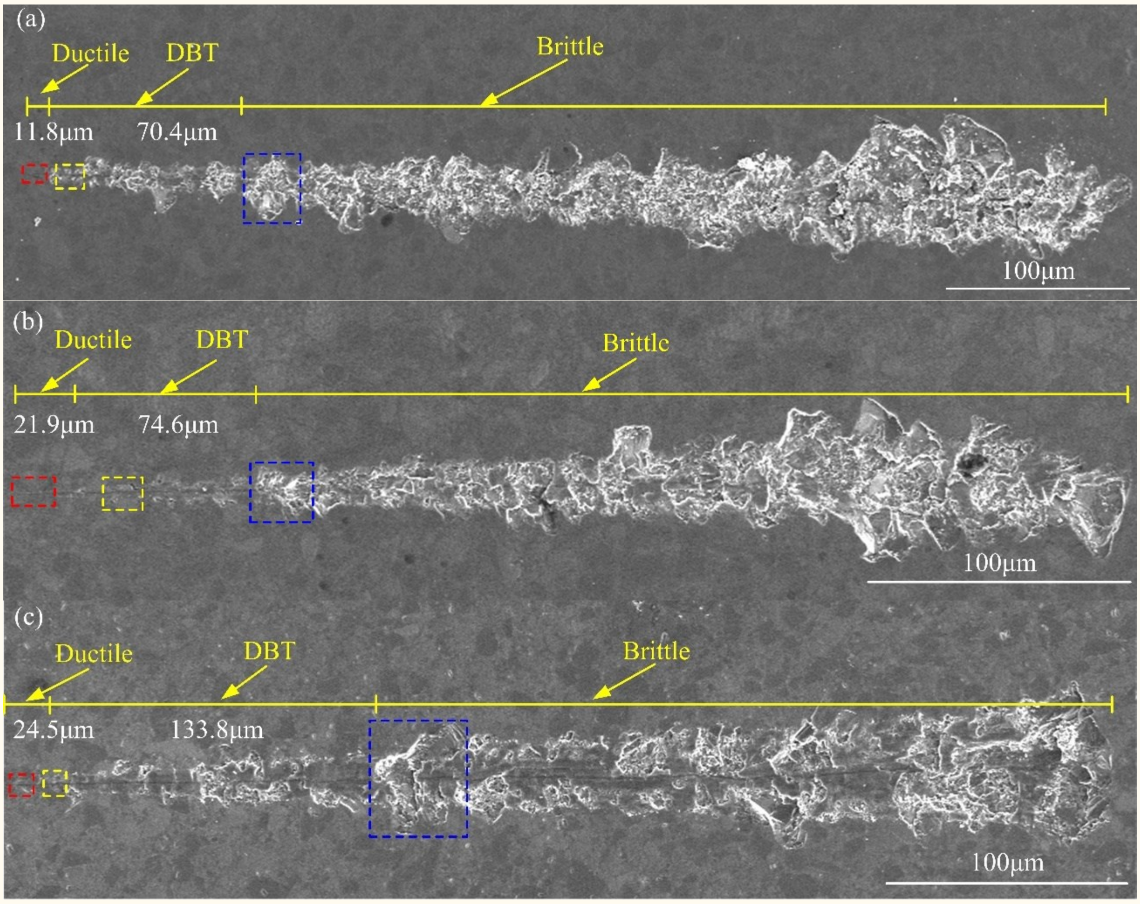

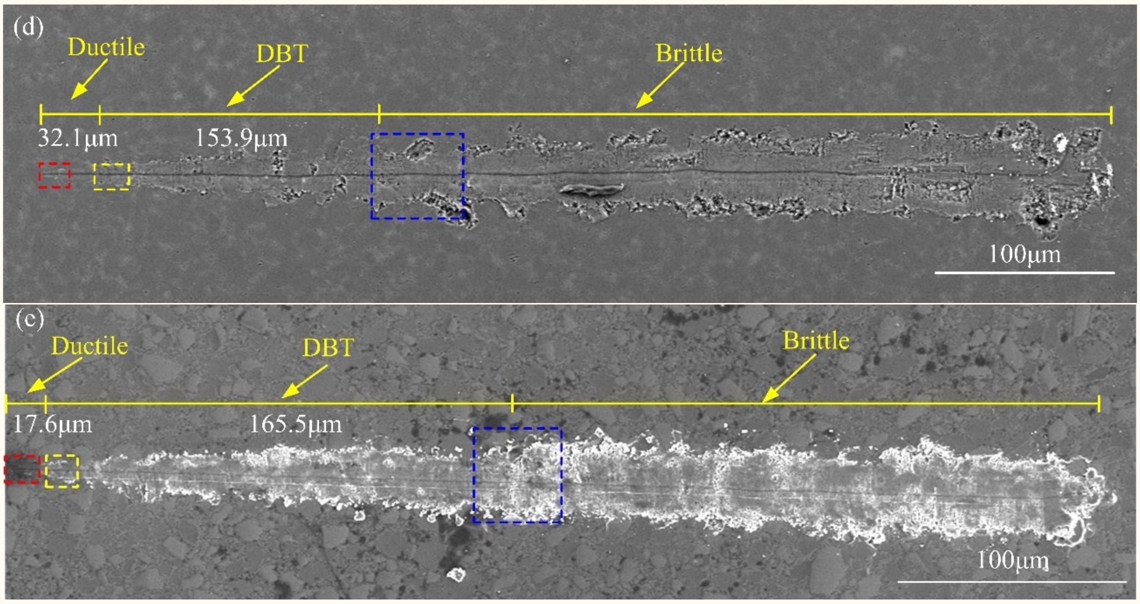

Fig. 3 SEM micrograph of the scratch grooves with linearly increased penetration depth at different temperatures. (a) RT, (b) 200℃, (c) 600℃, (d) 900℃ and (e) 1200℃.

In order to identify the morphology in different regimes at elevated temperatures, the detailed characteristics of the morphology were captured at the location in Fig. 3 marked with dotted boxes and were summarized in Table 3. The groove surface is smooth coupled with significant material pile-up on the sides in ductile regime. Fig.4 (a) shows the average heights of the material pile-up in ductile regime along the scratching direction measured by AFM. As observed in SEM images of the scratching grooves in Table 3, the material pile-up increases with the increase of temperatures, indicating the enhancement of plastic deformation. As a result, the measured scratching width increases because of the larger material pile-up at elevated temperature in ductile regime, shown in Fig.4 (b). Massive microcracks on the surface and minor fracture on the sides of the grooves are detected in the DBT regimes. When the temperature increases, the area of the fracture tends to decrease while the microcrack becomes obvious. In the brittle regime, a serious fracture occurs on both side and bottom of the grooves at room temperature and 200℃. With the increase of temperature, fracture in the valley of groove is converted into microcrack. Apparent track is then found on the bottom of groove at and above 600℃. The reduction in fracture ultimately results in the decrease of the measured scratching width in brittle regime above 600°C shown in Fig. 4 (b). This is because the dislocation is nearly immobile at and below 600°C while it is active above 600°C due to the DBT temperature [12], resulting in the gradual increase of plasticity in brittle regime above 600°C.

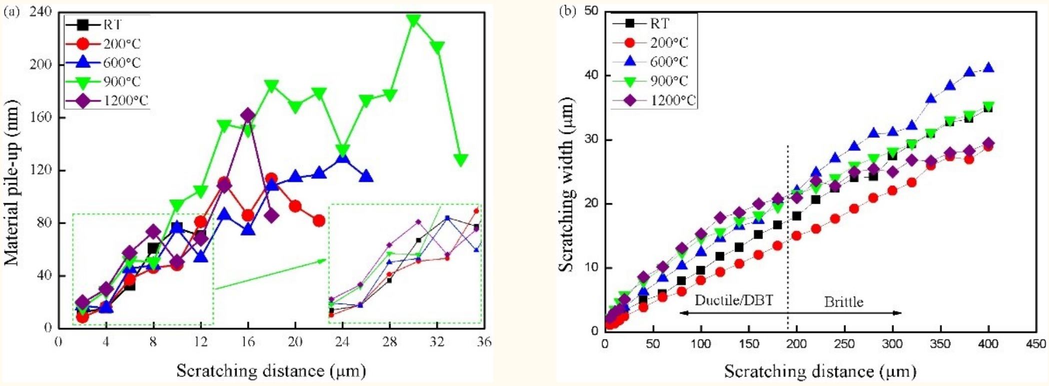

Fig. 4 Material pile-up and scratching width along the scratching distance (a) averages of the material pile-up in ductile regime and (b) scratching width in all regimes.

In addition, it is noteworthy that the material tearing, microcrack and fracture prefer to be generated at the grain boundary at all ambient temperatures. A similar result was also reported in Li et al.'s work [33]. RB-SiC ceramic is a typical polycrystalline workpiece including α-SiC, β-SiC and free Si [34]. The grains of SiC are oriented in different crystal orientations. The changes of grain orientation make the indenter experience the specimen with different crystallographic orientations and directions of cutting. Some of the grain boundaries cause the individual grains to slide along the easy cleavage direction and build-up of stresses at the grain boundaries [35]. Consequently, the different material removal modes of RB-SiC ceramics at elevated temperatures is easy to form at the grain boundary. All these changes in different regimes provide the direct evidences of the influence of heat on the material removal and the ductile-brittle transition of RB-SiC ceramics. Therefore, it is expected that the ductile removal of RB-SiC ceramics will be easier to achieve at a deeper cutting depth with the help of thermal process.

Table 3 Morphologies of the residual groove in different regimes at different temperatures

<table>
<tr><th>Tem.</th><th>Ductile regime</th><th>DBT regime</th><th>Brittle regime</th></tr>
<tr><td>RT</td><td>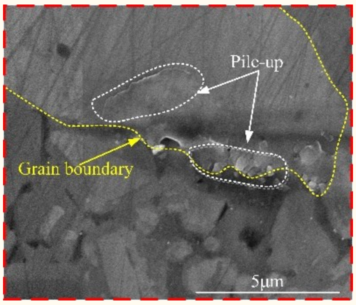
</td><td>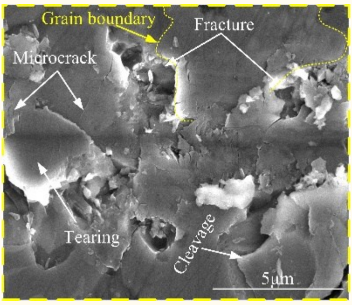
</td><td>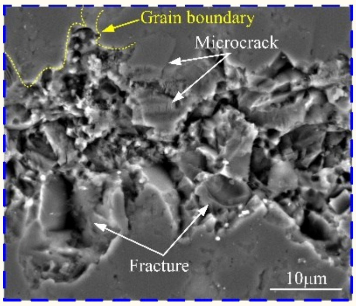
</td></tr>
<tr><td>200°C</td><td>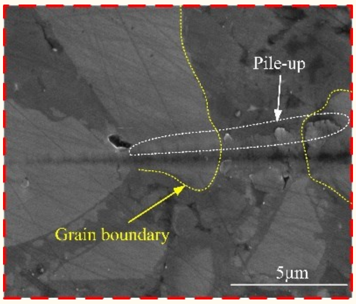
</td><td>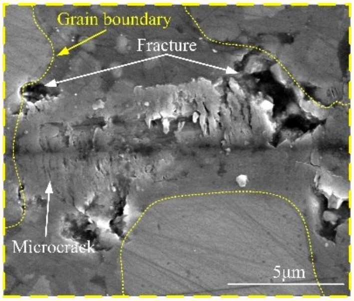
</td><td>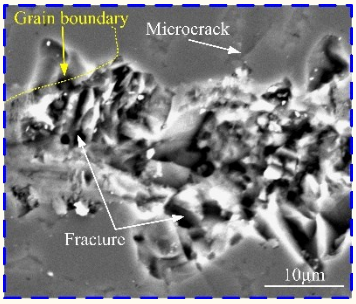
</td></tr>
<tr><td>600°C</td><td>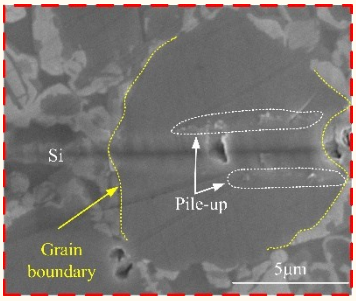
</td><td>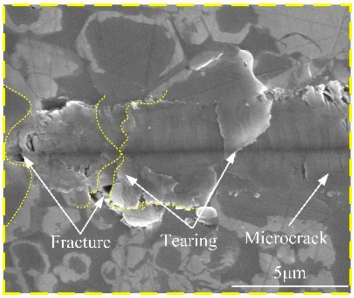
</td><td>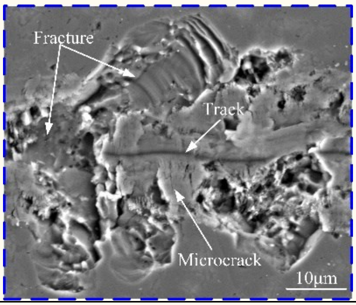
</td></tr>
<tr><td>900°C</td><td>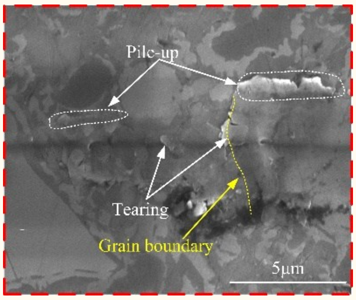
</td><td>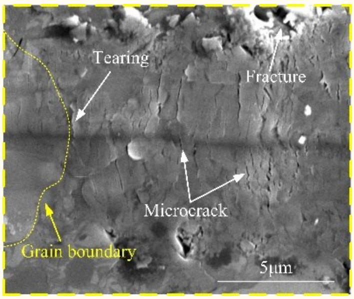
</td><td>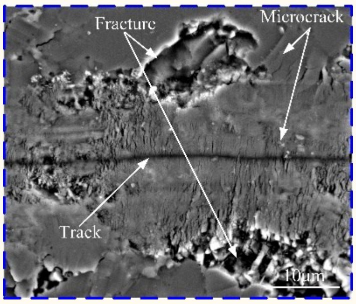
</td></tr>
<tr><td>1200°C</td><td>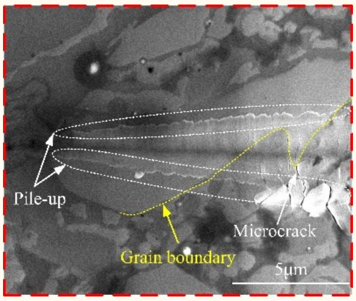
</td><td>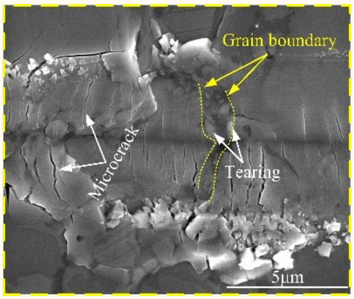
</td><td>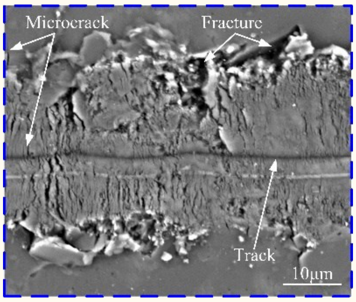
</td></tr>
</table>

3.2 Scratching hardness

Scratching hardness is considered as an indicator of the inherent material resistance to deformation in scratching process, which can be used to assess the material deformation of RB-SiC ceramic in different material removal regimes at elevated temperatures. By analogy with the static indentation hardness, the scratching hardness is defined as [36]:

$$H_s = \frac{P}{A_n} \tag{1}$$

Where P is the normal force and A_n is the normal projected area of the contact region. Due to the scratching direction was parallel to one diagonal of the indenter, only the two front faces of the indenter were kept in contact with the RB-SiC specimen during the scratching process shown in Fig.5 (a). Thus, the area of the projection can be deduced from the residual scratching width b regardless of the elastic deformation:

$$A_n = \frac{b^2}{4} \tag{2}$$

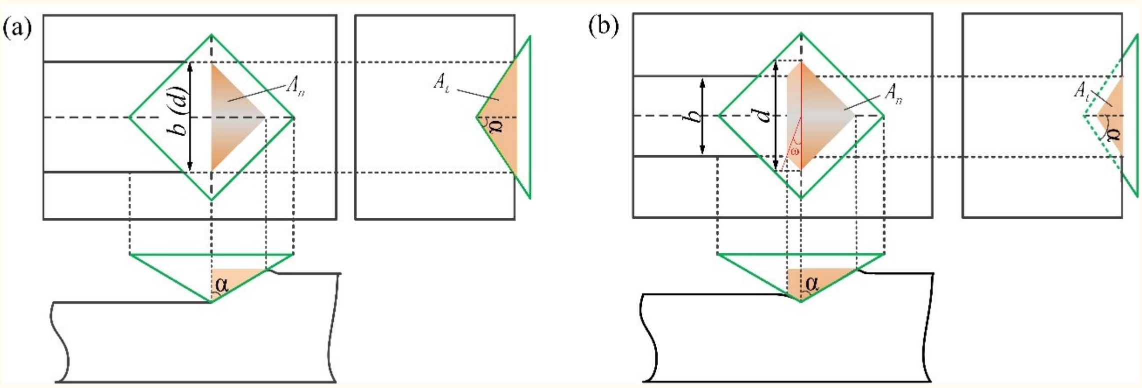

Fig. 5 Schematic of the contact area of the indenter during the scratching test. (a) the projection of the contact area for calculated scratching hardness (b) the projection of the actual contact area between the indenter and RB-SiC specimen in ductile regime considering the elastic deformation.

Fig. 6 (a) shows the scratching hardness along the scratching direction. These results present that the calculated scratching hardness decreases as the penetration depth increases along the scratching direction at all temperatures. As material is apt to undergo a ductile-brittle transition when subjected to a small infeed rate [35], the RB-SiC specimen is certainly suggested to remove in ductile regime at the beginning of the scratching process. The projection area of the actual contact region in Fig. 5 (b) is larger than the calculated contact area in Fig.5 (a) because of the elastic deformation. Consequently, a higher scratching hardness is obtained at the beginning of the scratching process. The scratching hardness decrease when the rigid-ductile/brittle regime become dominant, indicating a size effect similar to the indentation size effect phenomena observed in the Vickers indentation test [30]. Moreover, the scratching hardness tends to decrease with the increase of temperature, although it is slightly higher at 200°C than that at room temperature in brittle regime. The material plastic deformation is responsible for the decrease of the scratching hardness at elevated temperatures.

In order to gain insight of the material deformation of RB-SiC ceramics at elevated temperatures, the scratching hardness governed by the Meyer's law [30,37] was used to explain the size effect at elevated temperatures. By analogy with the evaluation of the indentation size effect in indentation test [38,39], the size effect in scratching test can be evaluated as:

$$P = Ab^n \tag{3}$$

Where constant A and Meyer's index n can be derived directly from the regression fitting of $\ln P$ (in Newton) versus $\ln b$ (in μm), plotted in Fig. 6 (b). The size effect can be evaluated by the deviation of the n-value from 2 [38]. It is evident that the size effect decreases because the index n is gradually close to 2 when the temperature increases, which indicates the increase of plastic deformation at elevated temperatures. Besides, the Meyer's indexes n_d and n_b were also calculated in ductile/DBT and brittle regimes respectively and summarized in Table 4. The increasing tendency of the Meyer's index with temperatures is owing to the decrease of elastic recovery [40], indicating the reduction in size effect induced by elastic deformation in ductile/DBT regime. In other words, the plasticity gradually dominates in material deformation of RB-SiC ceramics in ductile/DBT regime when the temperature increases, which is exactly the reason of the increase of material pile-up and scratching width at elevated temperatures observed in Section 3.1. In brittle regime, the decrease of the Meyer's index is attributed to material softening and deformation at elevated temperatures. The reason has been explicated in previous work [30]. Thus, the scratching hardness will have different load/depth-independent values because of the different roles that the plastic deformation plays in the scratching test at different temperatures.

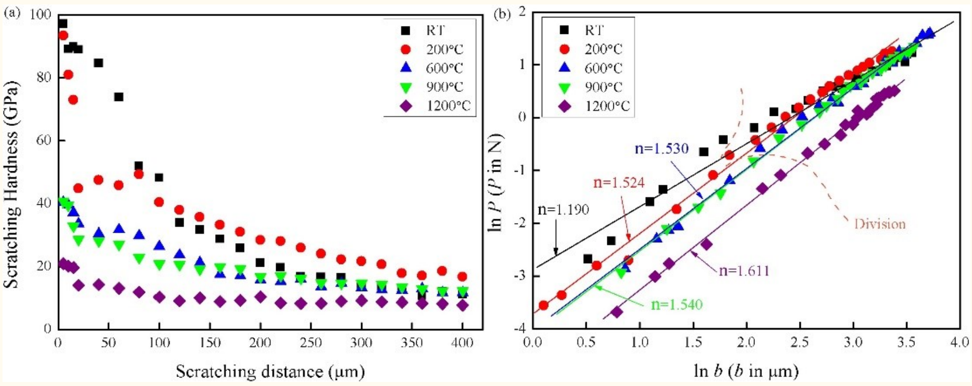

Fig.6 Analysis of the scratching hardness at different temperatures. (a) the calculated scratching hardness based on the measurements of scratching width (b) the size effect evaluated by Meyer's index.

Table 4 Meyer's index in ductile and brittle regimes at different temperatures

Temperature	Slope		
	n	n_d	n_b
RT	1.190	0.909	1.833
200°C	1.524	1.299	1.525
600°C	1.530	1.340	1.759

900°C	1.540	1.382	1.684
1200°C	1.611	1.585	1.669

The averages of scratching hardness in different regimes have been plotted in Fig.7 (a). A comparison has also been made between the scratching hardness and the load-independent Vickers hardness listed in Table 1. The results are summarized in Fig.7 (b). As expected, the scratching hardness decreases as the material removal transfers from ductile to brittle. Higher values of scratching hardness result from smaller residual scratching width induced by the elastic recovery in ductile regime. Meanwhile, the deviations of scratching hardness also reduce with the increase of temperatures in this transition. This is attributed to the enhanced plasticity at high temperatures [41].

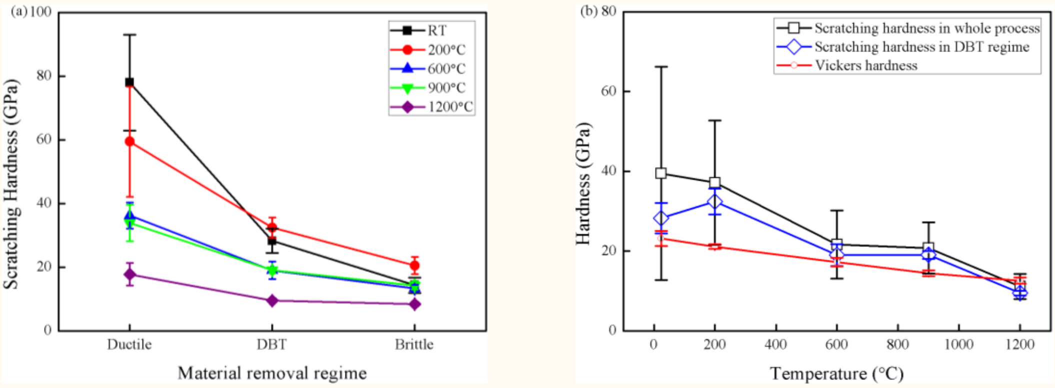

Fig. 7 The average of the scratching Hardness in different regimes at different temperatures. (a) the scratching hardness in different regimes (b) the averages of scratching hardness in DBT regime and whole process and the Vickers hardness.

In addition, it is interesting that the value of the scratching hardness in DBT regime is close to both that in whole process and that obtained in indentation test, which seems to suggest the elimination of the deviation on the scratching width induced by brittle fracture through plastic deformation. The scratching hardness in DBT regime has a slightly higher average than Vickers hardness at all temperatures except for 1200°C. This is attributed to the short loading time during the scratching test, whereas the hardness decreases at a longer loading time [42].

Higher value of the scratching hardness is hence obtained in the scratching tests. As a result, the scratching hardness in DBT regime can be treated as the depth-independent hardness at different temperature. It shows the reasonable application of the mechanical properties of RB-SiC ceramics obtained in Vickers indentation test in prediction of the critical depth of ductile-brittle transition in the scratching test.

3.3 Ductile-brittle transition

Based on the observation of the cracks and fracture generated on the bottom and sides of the residual groove, the transition of material removal mode from ductile to brittle fracture can be identified [43]. Therefore, the critical depth of ductile-brittle transition at different temperatures can be determined by combination of the observation on the morphology by SEM and AFM. The measurement results are summarized in Table 5. The corresponding cross-section profile at the location of ductile-brittle transition clearly unfolds the critical depth measured by AFM at different temperatures. It is clear that the critical depth of ductile-brittle transition has an increasing tendency of temperatures except for 1200℃. The critical depth of brittle material is usually considered relevant to its mechanical properties [44]. When the mechanical properties of RB-SiC ceramics at elevated temperatures such as elastic modulus, hardness and fracture toughness is taken into consideration, an interesting fact is found that the critical depth obtained in present work shows the same tendency as the variation of fracture toughness against temperatures. It implicates the most important role of fracture toughness in scratching of RB-SiC ceramics, which explicates the reduction in ductile regime scratching length at 1200°C abovementioned in Section 3.1. Therefore, the critical depth decreases again when the fracture toughness decrease due to the difficulty in resisting crack propagation because of the free Si softening in RB-SiC ceramics [45].

Table 5 The groove morphologies and corresponding cross-section profiles of ductile-brittle transition at different temperatures

Tem.	SEM	AFM	Cross-section profile
RT	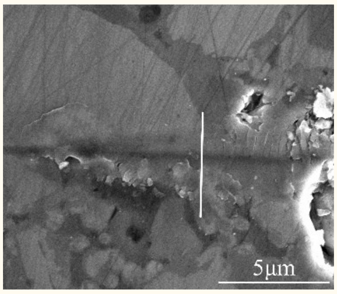	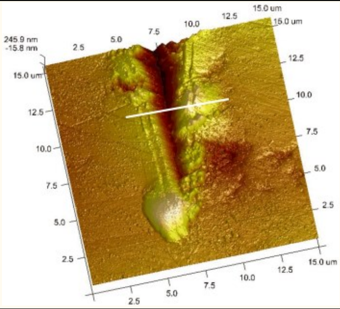	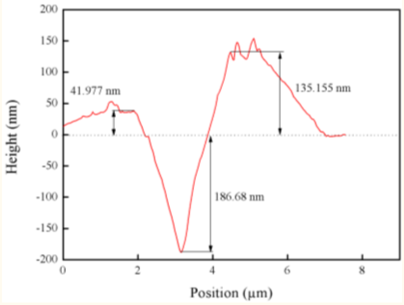
200℃	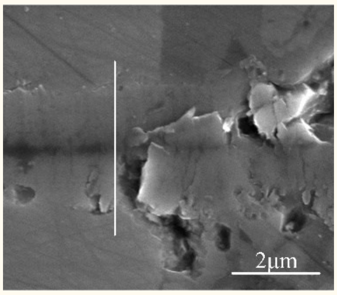	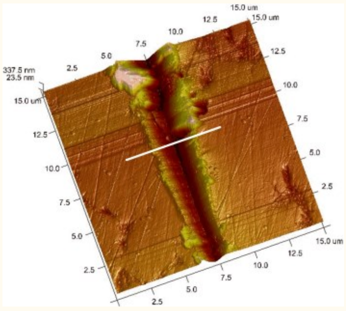	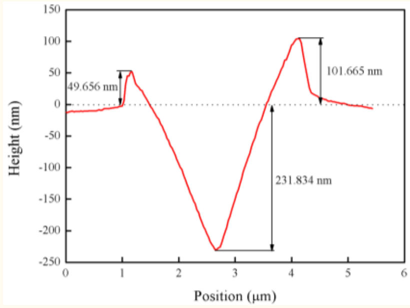
600℃	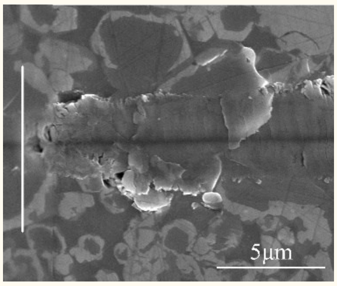	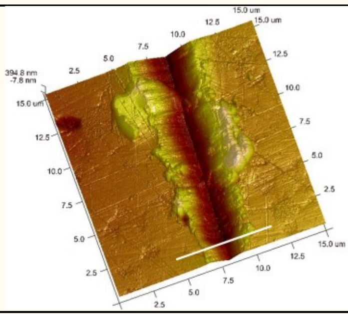	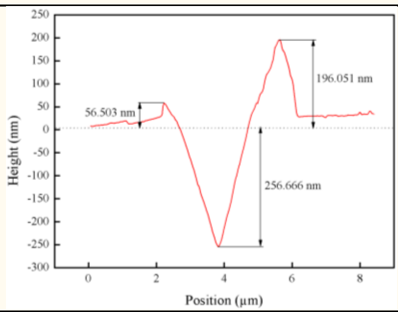
900℃	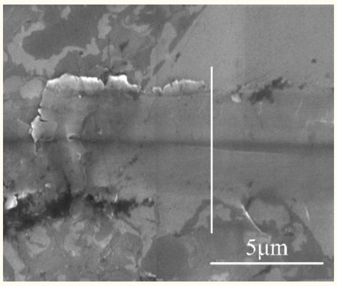	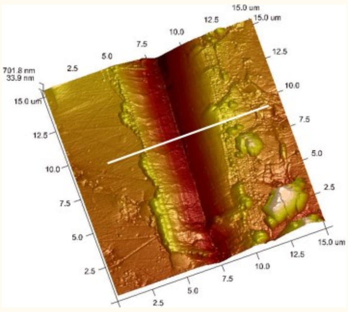	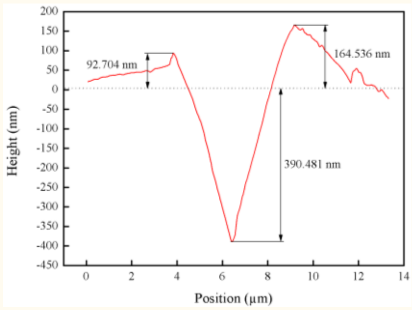
1200℃	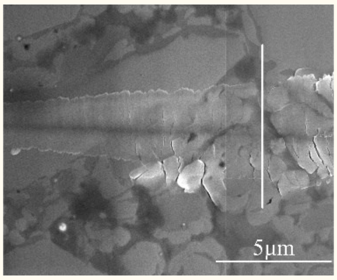	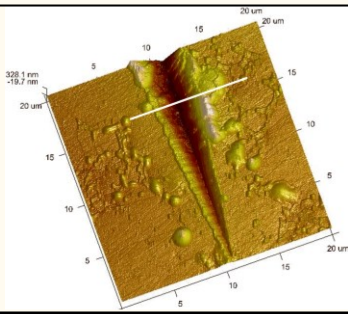	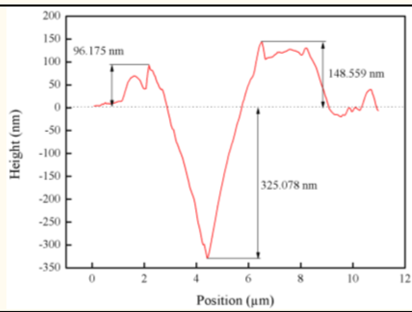

The relationship between the critical depth and the material properties is generally given by [46,47]:

$$h_c = \Psi\left(\frac{E}{H}\right)\left(\frac{K_c}{H}\right)^2 \tag{4}$$

Where E, H and K_C are the elastic modulus, hardness and fracture toughness of the material at a particular temperature, respectively. Ψ is a dimensionless constant dependent on indenter equivalent geometry, which is usually valued at 0.15 for Berkovich indenter [44,48]. However, this value has been proved to be unsuitable for the occasions in consideration of the size effect in obtaining material properties [49], the anisotropic characteristics of the specimen [47] and the effects of scriber tip geometry, friction etc [48]. Meanwhile, there is no report on Ψ at elevated temperatures. Thus, a reasonable Ψ needs to be determined by the experimental results, especially for those at elevated temperature because of significant variations in material properties. Without consideration of the constant Ψ, the relationship between the calculated critical depth and the measured critical depth at different temperatures is presented in Fig. 8(a). The ratios of the measured critical depth versus the calculated critical depth at different temperatures are also presented in Fig.8 (b).

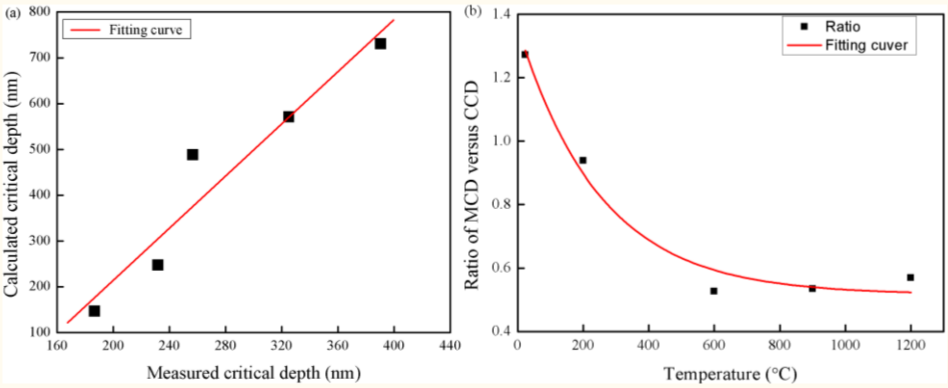

Fig.8 The calculated critical depth and measured critical depth. (a) relationship between the measured critical depth and calculated critical depth (b) ratio of measured critical depth (MCD) versus calculated critical depth (CCD) at different temperature.

It is evident that a reasonable correlation exists between the calculated critical depth and the measured critical depth because of their linear relationship at different temperatures [44]. A unique value of Ψ should be obtained without the influence of the temperature. However, the ratio of measured critical depth versus calculated critical depth shows a decreasing tendency when the temperature increases. By fitting, an exponential function of temperature is obtained for Ψ:

$$\Psi(T) = 0.52 + 0.85 exp(-T/T_0);\ T_0 = 251.1\,℃ \tag{5}$$

It is noteworthy that both the calculated critical depth and measured critical depth at room temperature and 200℃ are near the radius of the indenter tip (shown in Fig.1). In the case of microscale and nanoscale scratching, the influence of specific scratching energy induced by tip radius increase the critical depth of ductile-to-brittle transition [50,51]. As a result, higher ratio is obtained at room temperature and 200℃. Simultaneously, it should be noted that the $exp(-T/T_0)$ in equation (5) approaches zero at high temperatures and the ratio trends to a constant at and above 600℃. Then, the equation (4) for scratching test of RB-SiC ceramic at high temperature can be modified:

$$h_c = 0.52\left(\frac{E}{H}\right)\left(\frac{K_c}{H}\right)^2 \tag{6}$$

To validate the equation (6), more experiments with varied maximum scratching was arranged from 10μm to 30μm with increasement of 10μm. The averages of critical depth under different temperatures is shown in Fig.9. The maximum error between the predicted result and experimental result is only 4.95% at and above the temperature of 600℃.

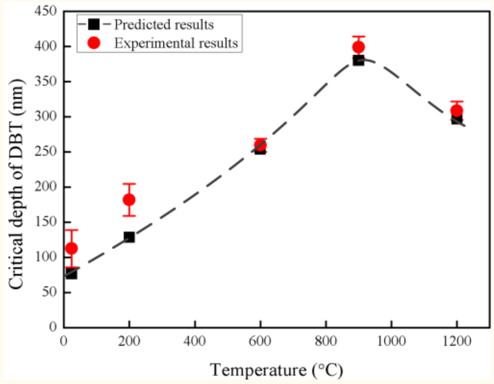

Fig. 9 The experimental results of critical depth for assessing accuracy of the modified model

3.4 Scratching force and friction behaviour

Fig. 10 shows the scratching forces at different temperatures. When the indenter penetrates into the specimen with linearly increased depth, the normal and thrust force gradually increases while the radial force keeps at zero because the two front faces of the indenter is symmetric as shown in Fig.10 (a). The fluctuation of the forces also increases because of the transition of material removal mode from ductile to brittle at all temperatures. Nevertheless, the fluctuating magnitude of the forces tends to reduce when the temperature increases. It indicates that high temperature facilities the ductile removal of the RB-SiC ceramics. Because more energy is consumed by ductile material removal and dislocations in brittle material are nearly immobile below the ductile-to-brittle transition temperature (less than $\approx \frac{1}{2}$ the melting temperature of the material) [12], the normal and thrust forces increase below the temperature of 700°C (about half of the melting temperature of the free Si in RB-SiC, which is 1410°C [2]). However, both the normal and thrust forces decrease again at 900°C and 1200°C owing to the plastic deformation of covalently bonded material in assistance of the active dislocation at higher temperatures [26]. The varied activity of dislocation at different temperatures will change the contact between the indenter and specimen, resulting in the different friction behaviour between them.

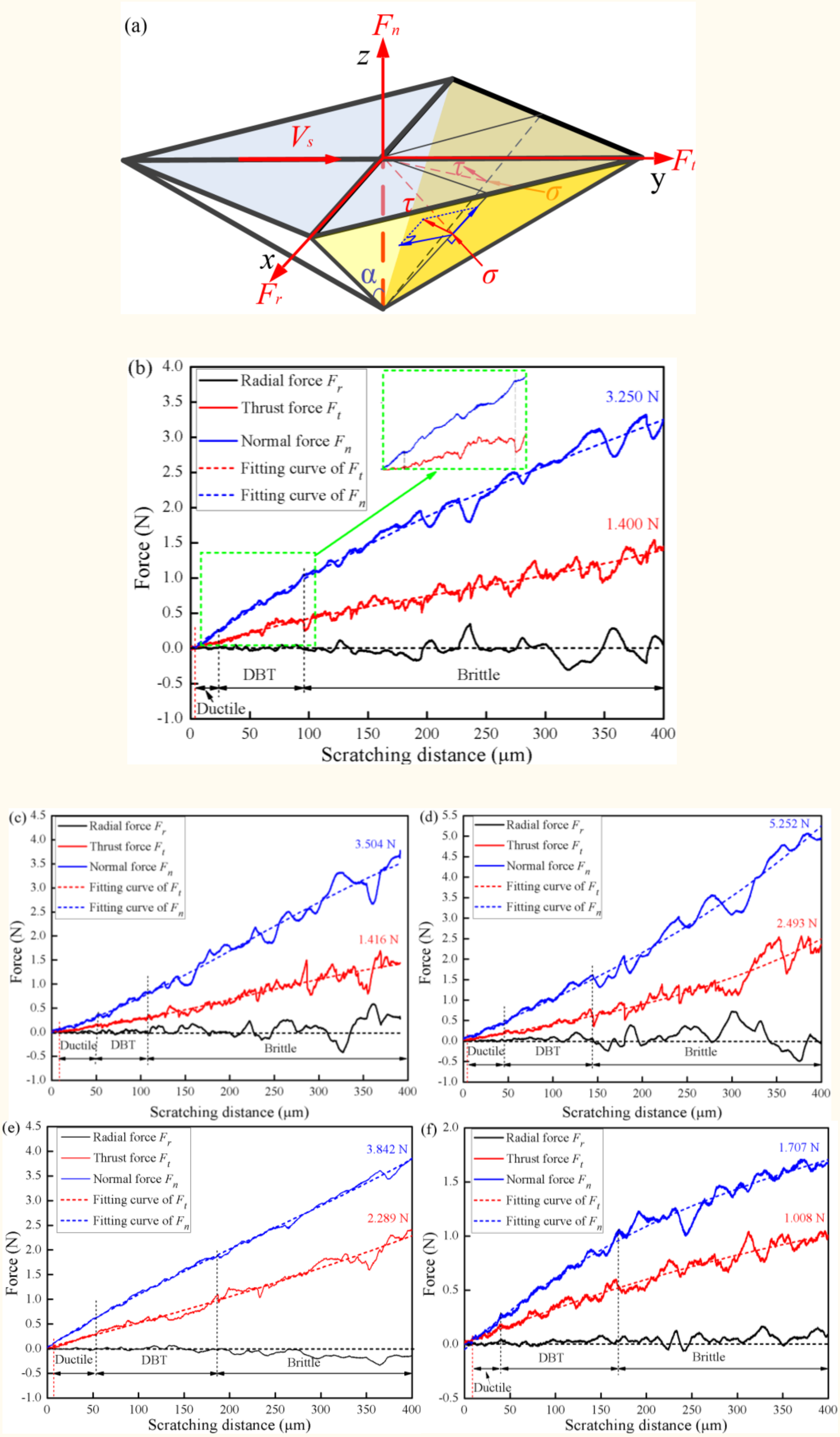

(a)
F_n
z
V_s
F_t
y
τ
σ
x
F_r
α
(b)
Radial force F_r
Thrust force F_t
Normal force F_n
Fitting curve of F_t
Fitting curve of F_n
3.250 N
1.400 N
DBT
Brittle
Ductile
Force (N)
Scratching distance (μm)
(c)
3.504 N
1.416 N
Ductile
DBT
Brittle
(d)
5.252 N
2.493 N
Ductile
DBT
Brittle
(e)
3.842 N
2.289 N
Ductile
DBT
Brittle
(f)
1.707 N
1.008 N
DBT
Brittle
Ductile

Fig.10 Scratching force at different temperature. (a) schematic diagram of loads on the two front faces of the indenter (b) Room temperature, (c) 200℃, (d) 600℃, (e) 900℃ and (f) 1200℃.

In general, the thrust force or 'friction' force is considered as the sum of the adhesion and ploughing terms in scratching test, namely [36]:

$$F_t = F_a + F_p \tag{7}$$

Where F_a and F_p are the adhesion force and ploughing force, respectively. Moreover, the ratio of ploughing force F_p to the projected area A_t (as shown in Fig.5) in the direction normal to the scratching direction of the indenter is defined as another value of the scratching hardness:

$$H_p = \frac{F_p}{A_t} \tag{8}$$

When it takes the elastic deformation into consideration (as shown in Fig.5 (b)), the projected area A_t can be determined by the geometric relationship while the normal projected area A_n should be rewritten as:

$$\begin{cases} A_n = \dfrac{d^2}{4}\left[2 - 1/(1 + \tan\omega)^2\right] \\ A_t = \dfrac{d^2}{4}\cot\alpha \Big/ (1 + \tan\omega)^2 \end{cases} \tag{9}$$

Where ω is the elastic recovery parameter with a range from $\pi/2$ to 0 when the material removal mode changes from ductile to brittle with the increase of penetration depth [27,52,53]. α is the half include angle between the opposite edges of the Vickers indenter shown in Fig.10 (a), which is 74°. Then, the overall coefficient of friction (COF) can be obtained by:

$$\mu = \frac{F_t}{F_\text{n}} = \frac{F_a}{F_n} + \frac{F_p}{F_n} \tag{10}$$

Note that the value of H_p is taken to be equal to the scratch hardness H_s [36]. Hence, combining Eq. (1), (8), (9) and (10), the overall COF can be rewritten as:

$$\mu = \mu_a + \frac{\cot\alpha}{2(1 + \tan\omega)^2 - 1} \tag{11}$$

Where $\mu_a = F_a/F_n$ is the adhesion term of the overall COF. However, the ploughing term of the overall COF depends on the elastic deformation during the scratching tests, which is given by the following equation according to Eq. (11):

$$\mu_p = \frac{\cot\alpha}{2(1 + \tan\omega)^2 - 1} \tag{12}$$

Therefore, the overall COF will vary with the transition of the material removal mode shown in Fig.11. As it can be seen, the overall COF sharply increases at temperatures below 900℃ while dramatically decreases at 1200℃ with the increase of penetration depth in ductile regime. As it is more important for ploughing relative to adhesion in ductile regime, material plastic deformation is responsible for the maximum values and initial curvatures of the ploughing COF [52]. The projected area A_t is negligible compared to the available contact area A_n when the elastic dominates in the regime [52,53], namely the limiting condition $\omega = \pi/2$, resulting in lower COF at the initial stage of the scratching process. Then the COF increases as result of the increase of plastic deformation when the penetration depth increases. Meanwhile, higher temperature facilitates significant material softening and plastic deformation of RB-SiC ceramics, leading to an ascending initial value of the COF at 1200℃. The dominant friction behaviour was even changed from ploughing to adhesion/rubbing at the initial stage of the scratching process because of the notable plastic deformation. As a result, the COF presents an extremely high value at the initial stage of the scratching process.

Note that the Eq. (12) tends to a constant at the limiting condition $\omega = 0$ when the brittle dominates the material removal. And the overall COF also tends to be stable after the ductile regime. It indicates that the adhesive COF is independent on the scratching depth in brittle regime. Thus, the adhesive COF can be determined for RB-SiC ceramics at a particular temperature, shown in Fig. 11 (f). Due to the material softening at high temperatures, the adhesive COF increases. Whereas it drops again at 1200℃ because of the oxidation of free Si in RB-SiC ceramics.

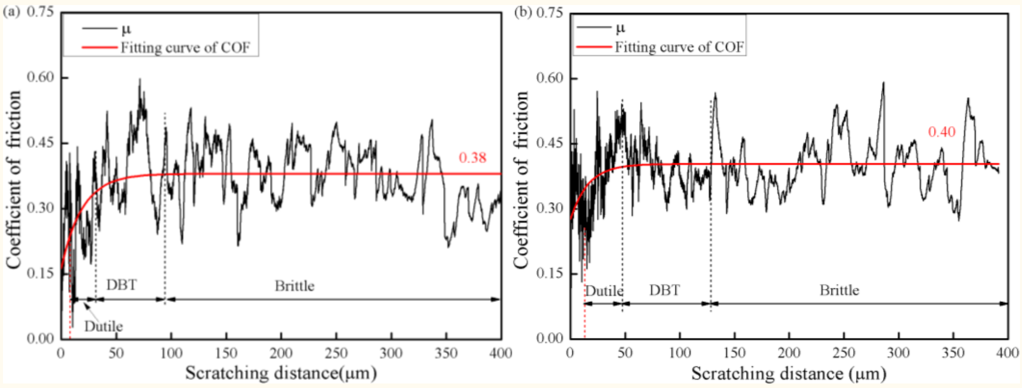

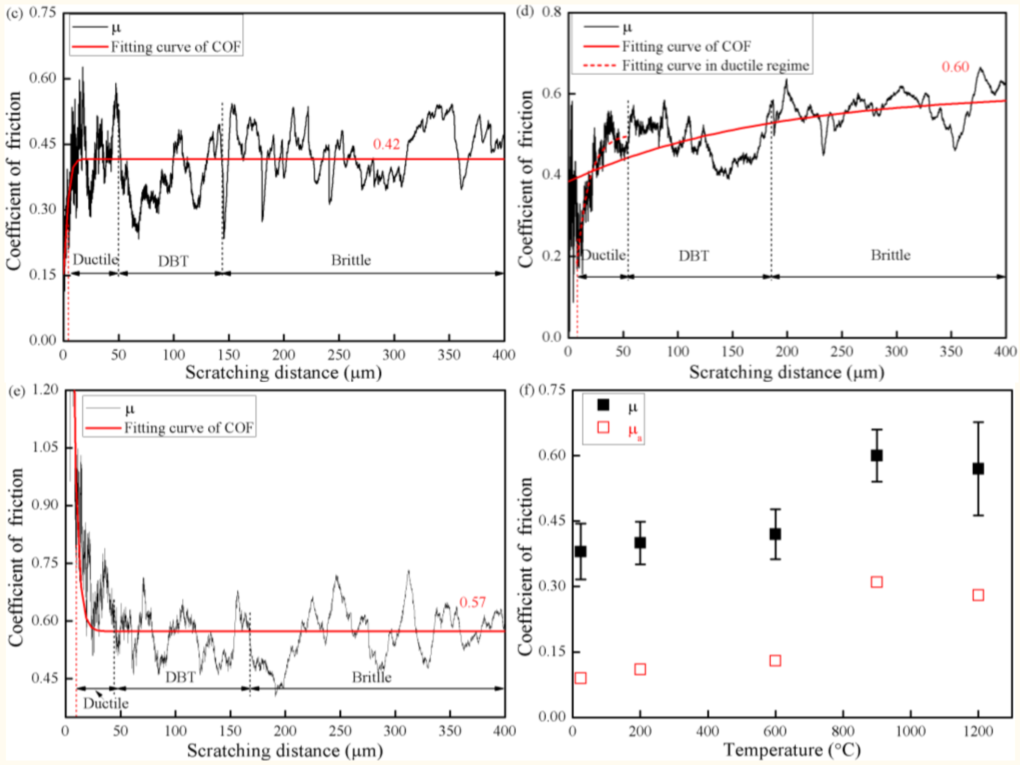

Fig. 11 Coefficient of friction at different temperatures. (a) Room temperature, (b) 200℃, (c) 600℃, (d) 900℃, (e) 1200℃ and (f) The overall and adhesion COFs varied with temperatures.

4. Conclusion

In present work, the scratching experiments were conducted to explore the influence of heat on the material removal and friction behaviour of RB-SiC ceramics under different temperatures. Three material removal regimes, scratching hardness, critical depth of ductile-brittle transition and the scratching force and corresponding COF were analyzed. The following conclusions were drawn:

(1) When the indenter penetrates the RB-SiC specimen gradually, the material removal undergoes ductile, ductile-to-brittle and brittle stages at all temperatures. The scratching length of the ductile regime increases from 11.8μm at RT to 31.1μm at 900℃, indicating high temperature facilitates the ductile removal of RB-SiC ceramics. The residual groove possesses smooth surface and material pile-up on the side formed in ductile regime. While minor fracture and mass microcrack are characteristics of residual groove formed

in DBT regime and fracture is the main characteristics of residual groove formed in brittle regime. The fracture in brittle regime dramatically decreases at and above 600℃ so that apparent track is observed at higher temperatures, providing the evidence for obtaining fine machined surface finish in ductile machining of RB-SiC ceramics with deeper penetration depth at elevated temperatures.

(2) Scratching hardness shows significant size effect similar to that in indentation test. Elastic recovery and plastic deformation are responsible for the size effects in ductile and brittle regimes, respectively. It is interesting to find that the average of scratching hardness in DBT regime is close to the hardness obtained in indentation test at all temperatures, which indicates that it is reasonable to predict the critical depth of brittle-ductile transition with the mechanical properties of RB-SiC ceramics obtained in indentation test. The scratching hardness decrease from 28.3±3.83GPa at RT to 9.8±0.56GPa at 1200℃, implying the ascending domination of plastic deformation at elevated temperatures.

(3) Critical depth initially increases from 186.68nm at RT to 390.48nm at 900℃ and then decreases to 325.08nm at 1200℃, showing a similar tendency of the fracture toughness with temperature obtained in indentation test. It indicates that the fracture toughness is the most important factor in controlling the critical depth at elevated temperatures. Simultaneously, material deformation of RB-SiC ceramics contributes to the increases of critical depth at high temperatures. A predictive model of critical depth with the maximum prediction error of 4.95% has been established on consideration of the changes of the mechanical properties of RB-SiC ceramics at elevated temperatures.

(4) The maximum normal scratching force of 5.25N occurs at 600℃ because of more energy consumption to ductile material removal and nearly immobile dislocation below 700℃. While it decreases to 1.71N at 1200℃ because the dislocation becomes active when the temperature is above 700℃. Meanwhile, the plastic deformation induced by material

dislocation makes the COF increase gradually from a lower value to a stable value in the ductile regime at temperature below 1200℃. When the temperature is 1200℃, the significant plastic deformation even changes the predominant friction behaviour from ploughing to adhesion/rubbing at the initial stage of the ductile regime. As the adhesive COF increases with the increase of temperatures, the overall COF increases from 0.38 at RT to 0.60 at 900℃ but drops to 0.57 because of the oxidation of free Si in RB-SiC at 1200℃.

Acknowledgements

This work was supported by the National Science and Technology Major Project of China (2018ZX04015001-005). The authors also gratefully acknowledge the financial support from the EPSRC (UK) (EP/K018345/1) and the International Cooperation Program of China (No. 2015DFA70630) for this study. We would like to express our gratitude to Dr. Wenlong Chang who has offered us valuable suggestions during our studies.

Date statement: All data underpinning this publication will be available from the University of Strathclyde KnowledgeBase at https://doi.org/10.15129/f038d90b-ca90-4c05-b955-0ccafd1f6f71

References

[1] S. Suyama, Y. Itoh, NTSIC (New-Technology Silicon Carbide): Evaluation of microstructure of high-strength reaction-sintered silicon carbide for optical mirror, Optical Materials and Structures Techbologies III, 6666 (2007) 66660K–66660K–11.

[2] W. Liu, L. Cheng, Y. Wang, H. Ma, Investigation of the residual stress in reaction-bonded SiC under irradiation, J. Eur. Ceram. Soc. 36 (2016) 3901–3907.

[3] J. Yan, Z. Zhang, T. Kuriyagawa, Tool wear control in diamond turning of high-strength mold materials by means of tool swinging, CIRP Ann. - Manuf. Technol. 59 (2010) 109–112.

[4] F. Ding, X. Luo, F. Zhang, Z. Li, Y. Cai, W. Chang, W. Zhong, Material removal mechanism of laser-assisted grinding of RB-SiC ceramics and process optimization, J. Eur. Ceram. Soc. 39 (2018) 705–717.

[5] X. Rao, F. Zhang, C. Li, Y. Li, Experimental investigation on electrical discharge diamond grinding of RB-SiC ceramics, Int. J. Adv. Manuf. Technol. 94 (2018) 2751–2762.

[6] Z. Dong, H. Cheng, Study on removal mechanism and removal characters for SiC and fused silica by fixed abrasive diamond pellets, Int. J. Mach. Tools Manuf. 85 (2014) 1–13.

[7] J. Xie, Q. Li, J.X. Sun, Y.H. Li, Study on ductile-mode mirror grinding of SiC ceramic freeform surface using an elliptical torus-shaped diamond wheel, J. Mater. Process. Technol. 222 (2015) 422–433.

[8] A.T. Akono, F.J. Ulm, Scratch test model for the determination of fracture toughness, Eng. Fract. Mech. 78 (2011) 334–342.

[9] K. Wasmer, C. Ballif, R. Gassilloud, C. Pouvreau, R. Rabe, J. Micher, J.M. Breguet, J.M. Solletti, A. Karimi, D. Schulz, Cleavage Fracture of Brittle Semiconductors from the Nanometre to the Centimetre Scale, Adv. Eng. Mater. 7 (2005) 309–317.

[10] B. Meng, F. Zhang, Z. Li, Deformation and removal characteristics in nanoscratching of 6H-SiC with Berkovich indenter, Mater. Sci. Semicond. Process. 31 (2015) 160–165.

[11] N. Duan, Y. Yu, W. Wang, X. Xu, SPH and FE coupled 3D simulation of monocrystal SiC scratching by single diamond grit, Int. J. Refract. Met. Hard Mater. 64 (2017) 279–293.

[12] J. Patten, W. Gao, K. Yasuto, Ductile Regime Nanomachining of Single-Crystal Silicon Carbide, J. Manuf. Sci. Eng. 127 (2005) 522–532.

[13] H. Pelletier, A.L. Durier, C. Gauthier, R. Schirrer, Viscoelastic and elastic-plastic behaviors of amorphous polymeric surfaces during scratch, Tribol. Int. 41 (2008) 975–984.

[14] A.T. Akono, F.J. Ulm, An improved technique for characterizing the fracture toughness via scratch test experiments, Wear. 313 (2014) 117–124.

[15] S. Lafaye, C. Gauthier, R. Schirrer, Analyzing friction and scratch tests without in situ observation, Wear. 265 (2008) 664–673.

[16] C. Pignie, M.G. Gee, J.W. Nunn, H. Jones, A.J. Gant, Simulation of abrasion to WC/Co hardmetals using a micro-tribology test system, Wear. 302 (2013) 1050–1057.

[17] V. Le Houérou, J.C. Sangleboeuf, S. Dériano, T. Rouxel, G. Duisit, Surface damage of soda-lime-silica glasses: Indentation scratch behavior, J. Non. Cryst. Solids. 316 (2003) 54–63.

[18] S. Kun Lee, R. Tandon, M.J. Readey, B.R. Lawn, Scratch Damage in Zirconia Ceramics, J. Am. Ceram. Soc. 83 (2004) 1428–1432.

[19] M.G. Gee, Low load multiple scratch tests of ceramics and hard metals, Wear. 250–251 (2001) 264–281.

[20] S. Gao, R.K. Kang, Z.G. Dong, B. Zhang, Z.G. Wang, Surface integrity and removal mechanism in grinding sapphire wafers with novel vitrified bond diamond plates, Mater. Manuf. Process. 32 (2017) 121–126.

[21] J. Wang, B. Guo, Q. Zhao, C. Zhang, Q. Zhang, W. Zhai, Evolution of material removal modes of sapphire under varied scratching depths, Ceram. Int. 43 (2017) 10353–10360.

[22] L. Tian, Y. Fu, J. Xu, H. Li, W. Ding, The influence of speed on material removal mechanism in high speed grinding with single grit, Int. J. Mach. Tools Manuf. 89 (2015) 192–201.

[23] C. Li, F. Zhang, X. Wang, X. Rao, Repeated nanoscratch and double nanoscratch tests of Lu2O3 transparent ceramics: Material removal and deformation mechanism, and theoretical model of penetration depth, J. Eur. Ceram. Soc. 38 (2018) 705–718.

[24] F. Petit, C. Ott, F. Cambier, Multiple scratch tests and surface-related fatigue properties of monolithic ceramics and soda lime glass, J. Eur. Ceram. Soc. 29 (2009) 1299–1307.

[25] Y. Zhang, C. Li, H. Ji, X. Yang, M. Yang, D. Jia, X. Zhang, R. Li, J. Wang, Analysis of grinding mechanics and improved predictive force model based on material-removal and plastic-stacking mechanisms, Int. J. Mach. Tools Manuf. 122 (2017) 81–97.

[26] P. Pirouz, On micropipes and nanopipes in sic and GaN, Philos. Mag. A Phys. Condens. Matter, Struct. Defects Mech. Prop. 78 (1998) 727–736.

[27] S. Lafaye, C. Gauthier, R. Schirrer, Analysis of the apparent friction of polymeric surfaces, J. Mater. Sci. 41 (2006) 6441–6452.

[28] J. Pujante, D. Casellas, M. Dolors, High temperature scratch testing of hard PVD coatings deposited on surface treated tool steel, Surf. Coat. Technol. 254 (2014) 352–357.

[29] M. Woydt, K.H. Habig, High temperature tribology of ceramics, Tribol. Int. 22 (1989) 75–88.

[30] X. Rao, F. Zhang, X. Luo, F. Ding, Characterization of hardness, elastic modulus and fracture toughness of RB-SiC ceramics at elevated temperature by Vickers test, Mater. Sci. Eng. A. 744 (2018) 426–435.

[31] M. Yang, C. Li, Y. Zhang, D. Jia, X. Zhang, Y. Hou, R. Li, J. Wang, Maximum undeformed equivalent chip thickness for ductile-brittle transition of zirconia ceramics under different lubrication conditions, Int. J. Mach. Tools Manuf. 122 (2017) 55–65.

[32] S.Z. Chavoshi, C.S. Gallo, H. Dong, X. Luo, High temperature nanoscratching of single crystal silicon under reduced oxygen condition, Mater. Sci. Eng. A. 684 (2017) 385–393.

[33] Z. Li, F. Zhang, X. Luo, Y. Cai, Fundamental understanding of the deformation mechanism and corresponding behavior of RB-SiC ceramics subjected to nano-scratch in ambient temperature, Appl. Surf. Sci. 469 (2019) 674–683.

[34] J.N. Ness, T.F. Page, Microstructural evolution in reaction-bonded silicon carbide, J. Mater. Sci. 21 (1986) 1377–1397.

[35] S. Goel, X. Luo, P. Comley, R.L. Reuben, A. Cox, Brittle-ductile transition during diamond turning of single crystal silicon carbide, Int. J. Mach. Tools Manuf. 65 (2013) 15–21.

[36] J. a Williams, Analytical rdness models of scratch, Tribol. Int. 29 (1996) 675–694.

[37] O. Franke, J.C. Trenkle, C.A. Schuh, Temperature dependence of the indentation size effect, J. Mater. Res. 25 (2010) 1225–1229.

[38] T.K. Roy, Assessing hardness and fracture toughness in sintered zinc oxide ceramics through indentation technique, Mater. Sci. Eng. A. 640 (2015) 267–274.

[39] J. Gong, J. Wu, Z. Guan, Examination of the indentation size effect in low-load vickers hardness testing of ceramics, J. Eur. Ceram. Soc. 19 (1999) 2625–2631.

[40] C.H. Kim, A.H. Heuer, A high-temperature displacement-sensitive indenter for studying mechanical properties of thermal barrier coatings, J. Mater. Res. 19 (2003) 351–356.

[41] R. He, Z. Qu, Y. Pei, D. Fang, High temperature indentation tests of YSZ coatings in air up to 1200 °C, Mater. Lett. 209 (2017) 5–7.

[42] S. Physics, Hardness and deformation properties of solids at very high temperatures, Proc. R. Soc. London. Ser. A. Math. Phys. Sci. 292 (1966) 441–459.

[43] A. Mir, X. Luo, J. Sun, The investigation of influence of tool wear on ductile to brittle transition in single point diamond turning of silicon, Wear. 364–365 (2016) 233–243.

[44] T.G. Bifano, T.A. Dow, R.O. Scattergood, Ductile-Regime Grinding: A New Technology for Machining Brittle Materials, J. Eng. Ind. 113 (1991) 184–189.

[45] Q.W. Huang, L.H. Zhu, High-temperature strength and toughness behaviors for reaction-bonded SiC ceramics below 1400 °c, Mater. Lett. 59 (2005) 1732–1735.

[46] P.N. Blake, R.O. Scattergood, Ductile-regime machining of germanium and silicon, J. Am. Ceram. Soc. 73 (1990) 949–957.

[47] J. Zhang, D. Wang, P. Feng, Z. Wu, C. Zhang, Material Removal Characteristics of KDP Crystal in Ultrasonic Vibration-Assisted Scratch Process, Mater. Manuf. Process. 31 (2016) 1037–1045.

[48] H. Wu, S.N. Melkote, Study of Ductile-to-Brittle Transition in Single Grit Diamond Scribing of Silicon: Application to Wire Sawing of Silicon Wafers, J. Eng. Mater. Technol. 134 (2012) 041011-1–8.

[49] Y.L. Sun, D.W. Zuo, H.Y. Wang, Y.W. Zhu, J. Li, Mechanism of brittle-ductile transition of a glass-ceramic rigid substrate, Int. J. Miner. Metall. Mater. 18 (2011) 229–233.

[50] S.H. Lee, Analysis of ductile mode and brittle transition of AFM nanomachining of silicon, Int. J. Mach. Tools Manuf. 61 (2012) 71–79.

[51] C.K. Ng, S.N. Melkote, M. Rahman, A. Senthil Kumar, Experimental study of micro- and nano-scale cutting of aluminum 7075-T6, Int. J. Mach. Tools Manuf. 46 (2006) 929–936.

[52] A.H. Carreon, P.D. Funkenbusch, Material specific nanoscratch ploughing friction coefficient, Tribol. Int. 126 (2018) 363–375.

[53] S. Lafaye, C. Gauthier, R. Schirrer, The ploughing friction: Analytical model with elastic recovery for a conical tip with a blunted spherical extremity, Tribol. Lett. 21 (2006) 95–99.